Calibration of multiple shunted piezoelectric transducers with correction for residual modes and shunt interactions

Jens Richardt, Boris Lossouarn, Jan Høgsberg, Jean-François Deü

Calibration of multiple shunted piezoelectric transducers with correction for residual modes and shunt interactions

Jens D. Richardt[1], Boris Lossouarn[2], Jan Høgsberg[1] and Jean-François Deü[2]

Abstract

Piezoelectric shunt damping can be used for efficient vibration mitigation of a single or multiple vibration modes of a structure. Several analytical tuning expressions have been derived for numerous circuit topologies for a single shunt. However, when multiple shunted piezoelectric transducers are attached to a flexible structure, their individual interactions alongside the spillover from residual modes affect the calibration accuracy. In this paper, explicit correction terms that represent these effects are presented for multiple shunted piezoelectric transducers targeting a single vibration mode. The correction terms are obtained from the evaluation of effective electromechanical coupling factors, while proper balancing between shunts follows from an assumed proportionality between shunt forces. The proposed correction method is applicable to general shunt architectures, for which tuning is available when targeting a single-degree-of-freedom structure. Its ability to regain nearby optimal damping properties is illustrated numerically for the classic series RL shunt.

Keywords

Piezoelectric shunt damping, resonant shunt calibration, residual mode correction, effective electromechanical coupling factor, vibration control

1 Introduction

Piezoelectric materials shunted with electrical circuits have been considered extensively for vibration control of flexible structures since the early work by Forward (1979), and Hagood and Von Flotow (1991). Several electrical circuits have been proposed for vibration control of one or multiple vibration modes. One simple circuit often used for single-mode vibration control is the so-called resonant (RL) shunt, where an inductance L is placed in series or parallel with a resistance R. This creates an electrical resonance that enables improved damping when tuned accurately to the natural frequency of a structure's most critical vibration mode (Hagood and Von Flotow 1991; Thomas et al. 2012).

Several calibration expressions have been derived for the calibration of the electrical components based on different objectives. For example, for the parallel and series RL shunt, explicit calibration methods are given by e.g. Hagood and Von Flotow (1991), Wu (1996), Caruso (2001), Høgsberg and Krenk (2012), Yamada et al. (2010), Thomas et al. (2012), Soltani et al. (2014), Soltani et al. (2017), and Ikegame et al. (2019). The majority of the presented calibration methods are derived for a single shunt in a lumped two-dof model, which couples the single RL shunt resonance with the structures' dominant vibration mode. However, as shown by Gardonio and Casagrande (2017) for a single piezoelectric shunt on a two-dimensional plate, accurate shunt calibration must account for the influence of residual modes. In the last decade, several methods have been proposed to correct the influence of residual modes for calibration of a single resonant vibration absorber. A quasi-static correction for the influence of residual modes by a supplemental flexibility term is introduced in Krenk and Høgsberg (2014) for mechanical vibration absorbers and extended to piezoelectric vibration absorbers by Høgsberg and Krenk (2015). A similar correction for the influence of higher modes on piezoelectric vibration absorbers is proposed in Berardengo et al. (2016b) by a correction of the inherent capacitance. A more general correction for residual modes by a quasi-dynamic correction with inertia and flexibility terms is presented for mechanical vibration absorbers in Krenk and Høgsberg (2016) and for resonant

[1]Department of Civil and Mechanical Engineering, Technical University of Denmark, Kongens Lyngby, Denmark
[2]Laboratoire de Mécanique des Structures et des Systèmes Couplés, Conservatoire national des arts et métiers, Paris, France

Corresponding author:
Jens D. Richardt, Department of Civil and Mechanical Engineering, Technical University of Denmark, Kongens Lyngby, Denmark.
Email: jdari@dtu.dk

piezoelectric shunts in Høgsberg and Krenk (2017). Toftekær et al. (2018) has recently shown, that residual-mode effects can almost exactly be accounted for by simply using the effective electromechanical coupling factor (EEMCF) in piezoelectric shunt tuning.

Besides being affected by residual modes, the tuning of multiple shunts is also affected by the interaction between shunts. However, there is limited literature on how this interaction affects the shunt calibration. Recently, Toftekær and Høgsberg (2020) considered the calibration of multiple RL shunts, where a modal capacitance for each shunt, in combination with an assumed voltage ratio between the shunts, encapsulates the influence from both residual modes and shunt interactions. The presented modal capacitance deliberately ignores any coupling effects of the shunts by residual modes, which leads to simple calibration terms. Trindade et al. (2021) compared parametric uncertainties of multiple decentralized RL shunts and multiple piezoelectric patches connected to an electrical network targeting a single mode. A uniform calibration method for multiple decentralized shunts and multiple piezoelectric patches connected to a network has been considered by Raze et al. (2022) with residual modes included by a modal electromechanical coupling factor. Furthermore, calibration of multiple shunts targeting a single mode has been addressed for periodic structures and metamaterials in e.g. Thorp et al. (2001), Casadei et al. (2009), Lossouarn et al. (2015), and Airoldi and Ruzzene (2011).

The present paper derives explicit correction terms that consistently include the influence from both residual modes and shunt interaction in the tuning of multiple shunted piezoelectric transducers. The correction terms are applicable for any shunt circuit targeting a single vibration mode. The presented work is a comprehensive extension of the conference paper by Richardt et al. (2023).

Optimal vibration mitigation can be realized for multiple shunted piezoelectric transducers targeting a single vibration mode by distributing the shunt resonances individually around the targeted frequency, as shown for multiple tuned mass dampers by Abé and Fujino (1994), Igusa and Xu (1994) and Yang et al. (2022). However, this tuning principle relies on numerical and thus non-explicit optimization. In this paper, an alternative balancing of the shunts is therefore applied. The interaction between shunts is represented by a force ratio associated with the limiting case of all shunts in open-circuit (OC) conditions. This force proportionality allows for explicit correction terms and corresponds to all shunts operating in phase for uni-modal excitation, a desired property derived by Main and Krenk (2005) for multiple viscous dampers and applied to multiple tuned mass dampers in Hoffmeyer and Høgsberg (2020) by scaling of the absorber mass. A similar concept has been applied for resonant piezoelectric shunts by Toftekær and Høgsberg (2020), where the interaction between the shunts is only included for the targeted vibration mode to be damped. The main novelty of the present paper is the inclusion of shunt interaction, both for the target mode as well as for the residual modes, while allowing for free sizing of the shunts' inherent capacitance.

The structure of the paper is as follows: Section 2 describes the mechanical and electrical models with respect to a modal expansion with all shunts in short-circuit (SC) conditions, while in Section 3, the effects of residual modes are accounted for by the evaluation of EEMCFs. Then, the interaction between multiple shunts targeting a single vibration mode is included in Section 4, resulting in the formulation of explicit correction terms. A numerical example in Section 5 demonstrates the accuracy of the proposed correction method for the series RL-shunt, chosen due to its wide use and large sensitivity to even small perturbations in the electrical parameters (Gripp and Rade 2018; Andreaus and Porfiri 2007; Wu 1996; Berardengo et al. 2016a; Trindade et al. 2021). Finally, conclusions are presented in Section 6.

2 Multiple shunts targeting a single mode

Piezoelectric shunts can be tuned to target a single frequency. This section derives the governing equations and expressions for the mechanical structure, the electrical shunt and the electromechanical coupling for multiple piezoelectric shunts targeting the same frequency.

2.1 Governing equations

Consider a discretized model of a flexible structure, with N degrees of freedom and P piezoelectric shunts attached. Figure 1 shows the free-free rod with $P = 20$ piezoelectric shunts used as a numerical example in Section 5. The P piezoelectric transducers are each shunted to a decentralized electrical circuit, with the charge Q_p and the voltage V_p across the electrodes of the p'th shunt. A modal expansion is introduced for the discretized model with all shunts in SC, i.e. $V_p = 0$ for $p = 0 \dots P$. The generalized displacements

$$\mathbf{q} = \sum_{n=1}^{N} \mathbf{u}_n r_n \tag{1}$$

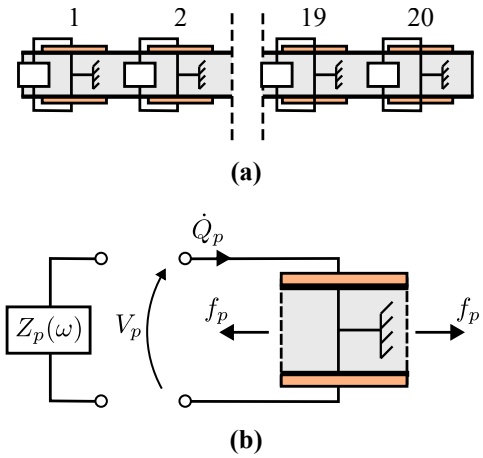

Figure 1. A free-free rod with 20 equally distributed piezoelectric shunts. Distribution of the shunts on the rod **(a)**. Individual impedance Z_p and supplementary force f_p for each shunt p **(b)**.

are hereby expressed by the modal coordinate r_n and the corresponding mode shape vector $\mathbf{u}_n$ for a mode n.

The governing equations for the n'th vibration mode are expressed for harmonic motion with angular frequency ω. Structural damping and external loading are not included in the subsequent shunt tuning. In accordance with Thomas et al. (2009); Berardengo et al. (2016b), and derivations in Appendix A and B, the electromechanical system is governed by the equations

$$\left(-\omega^2 m_n + k_n\right) r_n + \sum_{p=1}^{P} \nu_{n,p} f_p = 0 \tag{2}$$

$$Q_p = \theta_p \sum_{n=1}^{N} \nu_{n,p} r_n + C_p V_p \tag{3}$$

where m_n is the modal mass, k_n is the modal stiffness, $\nu_{n,p}$ represents the deformation of the mode shape vector $\mathbf{u}_n$ along the p'th piezoelectric transducer (defined in Appendix B), f_p is the force of the p'th piezoelectric shunt acting on the structure, while θ_p and C_p are the corresponding piezoelectric coefficient and blocked capacitance, respectively.

For each piezoelectric shunt, the associated shunt force

$$f_p = -\theta_p V_p \tag{4}$$

is proportional to the voltage V_p across its electrodes. The charge Q_p and the associated current $I_p = i\omega Q_p$ are governed by the voltage V_p via the frequency-dependent impedance $Z_p = Z_p(\omega)$ through the relations

$$V_p = -Z_p I_p = -i\omega Z_p Q_p \tag{5}$$

Inserting (4) and (5) into (3) leads to the modal force-displacement relationship

$$\left(\frac{C_p}{\theta_p^2} + \frac{1}{i\omega}\frac{1}{\theta_p^2 Z_p}\right) f_p = \sum_{n=1}^{N} \nu_{n,p} r_n \tag{6}$$

for an arbitrary shunt p. The electromechanical system is now governed by N modal equations of motion in (2), coupled to P force-displacement relations in (6). The modal interaction between the two sets of equations is represented by the two summations, in which the modal normalization is accounted for by $\nu_{n,p}$ defined in (B.3).

2.2 Governing electromechanical equation

The modal equation of motion (2) and the modal force-displacement relationship in (6) can be merged to form a single combined equation for each target shunt $p = t$ and the targeted structural vibration mode $n = s$.

Initially, the modal coordinate r_n for a general mode n is isolated as

$$r_n = -\sum_{p=1}^{P} \frac{\nu_{n,p} f_p}{-\omega^2 m_n + k_n} \tag{7}$$

from the modal equation of motion (2). This expression demonstrates the influence of the P shunts on the individual vibration modes. In case $\nu_{n,t} = 0$, for a specific shunt $p = t$ in (7), the contribution from that shunt to mode n vanishes because the transducer t is located at a nodal point of mode n.

Upon substitution of expression (7) for r_n, the modal force-displacement relationship (6) can be expressed as

$$\left(\frac{C_t}{\theta_t^2} + \frac{1}{i\omega}\frac{1}{\theta_t^2 Z_t}\right) f_t + \sum_{p=1}^{P}\sum_{n=1}^{N} \frac{\nu_{n,t}\nu_{n,p} f_p}{-\omega^2 m_n + k_n} = 0 \tag{8}$$

for a specific shunt $p = t$. In this relation, the summation across both modes n and shunts p comprise the influence from residual mode spill-over and shunt interaction.

In the following, the piezoelectric shunts are all calibrated to target a single vibration mode $n = s$, with the SC natural angular frequency

$$\omega_s = \sqrt{\frac{k_s}{m_s}} \tag{9}$$

obtained directly from the eigenvalue problem in (B.1). The relation for shunt t in (8) is conveniently rewritten by separating the targeted mode $n = s$ from the residual modes $n \neq s$. By introducing the SC natural frequency from (9) and multiplying the entire equation by $1/\nu_{s,t}$, the governing equation (8) for shunt force f_t with respect to target mode

$n = s$, can then be expressed in the homogeneous form

$$\sum_{p=1}^{P} \left(\frac{1}{\kappa_{tp}} + \delta_{tp} \frac{1}{i\omega} \frac{k_s}{\nu_{s,t}\nu_{s,p}\theta_t^2 Z_t} - \frac{\omega_s^2}{\omega^2 - \omega_s^2} \right) \frac{\nu_{s,p} f_p}{k_s} = 0 \tag{10}$$

where δ_{tp} is the Kronecker's delta that allows shunt t to be included within the summation. The effective stiffness ratio κ_{tp} is conveniently expressed by the reciprocal relation

$$\frac{1}{\kappa_{tp}} = \delta_{tp} \frac{k_s C_t}{\nu_{s,t}\nu_{s,p}\theta_t^2} + \sum_{n \neq s}^{N} \frac{\nu_{n,t}\nu_{n,p}}{\nu_{s,t}\nu_{s,p}} \frac{k_s}{-\omega^2 m_n + k_n} \tag{11}$$

where the first term represents the direct stiffness from the inherent capacitance of the t'th transducer, while the remaining terms within the summation account for the apparent dynamic stiffness from residual modes.

For multiple shunts $(P > 1)$, the first and last terms in (10) include the influence from the presence of other shunts, previously referred to as shunt interaction, because they prevail when $p \neq t$. Furthermore, the effective stiffness ratio κ_{tp} in (11) contains both the blocked piezoelectric capacitance C_t as well as a summation across all residual modes. Thus, the present representation consistently includes the influence of residual modes and interaction between the shunts. In the following sections, the summation of residual modes in (11) is considered as a quasi-static term, similar to the correction in Krenk and Høgsberg (2014) and Høgsberg and Krenk (2015). The quasi-static correction terms are then condensed into a set of EEMCFs by considering the shunts' OC limits.

3 Effective stiffness ratio and EEMCF

The effective stiffness ratio κ_{tp} defined in (11) contains a summation of all residual modes, not targeted by the shunts. Although exact, this direct evaluation of the summation is not applicable to larger numerical models. Therefore, this section approximates the effective stiffness ratio κ_{tp} by a set of generalized EEMCFs, obtained by switching shunts individually or pairwise into OC. In the following, it is assumed that κ_{tp} is frequency-independent, which is a valid approximation in engineering applications that typically exhibit small changes in frequency when switching from SC to OC electrodes.

3.1 All shunts in OC

It follows from (4) that $f_p = 0$ when the shunt p is in SC ($V_p = 0$). The associated SC natural frequency ω_s in (9) for target mode $n = s$ is obtained by solving the fundamental eigenvalue problem in (B.1). When changing from SC to OC, the vanishing charge $Q_p = 0$ in shunt p corresponds to $Z_p \to \infty$, whereby (A.3) depicts an apparent increase in stiffness that can be measured indirectly by the associated increase in natural frequency.

An ultimate limit occurs when all shunts $p = 1 \dots P$ are in OC, whereby $Z_p \to \infty$. The corresponding eigenvalue problem is given in (B.4) with $\hat{\mathbf{u}}_n$ and $\hat{\omega}_n$ denoting the n'th mode shape and natural frequency, respectively.

The EEMCF can be defined as for a single shunt in e.g. Hagood and Von Flotow (1991); Caruso (2001); Thomas et al. (2012); Berardengo et al. (2016b), namely by the relative increase in natural frequency squared,

$$K^2 = \frac{\hat{\omega}_s^2 - \omega_s^2}{\omega_s^2} \tag{12}$$

This EEMCF represents the P shunts' ultimate level of electromechanical coupling for the target mode $n = s$. A partial coupling effect is realized when only switching some $(< P)$ of the shunts from SC to OC. In the remainder of this section, such partial EEMCFs are used to estimate the effective stiffness ratios κ_{tp} defined in (11).

3.2 Single shunt in OC

The diagonal effective stiffness ratios κ_{tt} are seen from (11) to include both the apparent stiffness from the inherent capacitance (first term) as well as the residual mode contributions from other modes (remaining terms inside summation). When all other shunts than $p = t$ are in SC, the shunt forces $f_p = 0$ for $p \neq t$. Combined with $Z_t \to \infty$ for shunt t in OC, the governing equation in (10) reduces to

$$\left(\frac{1}{\kappa_{tt}} - \frac{\omega_s^2}{\omega^2 - \omega_s^2} \right) \frac{\nu_{s,t} f_t}{k_s} = 0 \tag{13}$$

which constitutes the characteristic equation for the single shunt t in OC and the remaining shunts in SC. The associated natural frequency $\omega = \hat{\omega}_{s,tt}$ for mode s with the shunt t in OC is obtained by solving the eigenvalue problem (B.5). The index tt in $\hat{(\,)}_{s,tt}$ refers to its direct relation with the diagonal effective stiffness ratio κ_{tt}.

As the characteristic equation in (13) governs the natural frequency for mode $n = s$ with the single shunt $p = t$ in OC and the remaining shunts in SC, the solution to the characteristic equation must be $\omega = \hat{\omega}_{s,tt}$. Thus, the diagonal effective stiffness ratio can be isolated in (13) as

$$\kappa_{tt} = \frac{\hat{\omega}_{s,tt}^2 - \omega_s^2}{\omega_s^2} = K_{tt}^2 \tag{14}$$

which defines the EEMCF K_{tt}^2 associated with shunt t in OC relative to all shunts in SC. A similar definition of the EEMCF is used in Thomas et al. (2009) for a single shunt attached to a structure with multiple shunts.

3.3 Shunt pairs in OC

The off-diagonal (or coupling) effective stiffness ratios κ_{tp} (for $p \neq t$) in (10) are now determined by a similar approach to that in the previous Section 3.2, just with two shunts t and p in OC and all other shunts in SC. The governing equation (10) can be written for shunt $p = t$ and $p = k$, with both shunts in OC and all other shunts in SC, using the relation $f_p = 0$ for $p \neq k, t$ and both Z_k and $Z_t \to \infty$. When changing index k back to p, the two homogeneous relations for f_t and f_p can be written in matrix form as

$$\begin{bmatrix} \frac{1}{\kappa_{tt}} - \frac{\omega_s^2}{\omega^2 - \omega_s^2} & \frac{1}{\kappa_{tp}} - \frac{\omega_s^2}{\omega^2 - \omega_s^2} \\ \frac{1}{\kappa_{tp}} - \frac{\omega_s^2}{\omega^2 - \omega_s^2} & \frac{1}{\kappa_{pp}} - \frac{\omega_s^2}{\omega^2 - \omega_s^2} \end{bmatrix} \begin{bmatrix} \frac{f_t \nu_{s,t}}{k_s} \\ \frac{f_p \nu_{s,p}}{k_s} \end{bmatrix} = \begin{bmatrix} 0 \\ 0 \end{bmatrix} \tag{15}$$

where symmetry $\kappa_{pt} = \kappa_{tp}$ is implied. A non-trivial solution to (15) requires the determinant of the coefficient matrix to vanish, which gives the characteristic equation

$$\left(\frac{1}{\kappa_{tt}} - \frac{\omega_s^2}{\omega^2 - \omega_s^2} \right) \left(\frac{1}{\kappa_{pp}} - \frac{\omega_s^2}{\omega^2 - \omega_s^2} \right) - \left(\frac{1}{\kappa_{tp}} - \frac{\omega_s^2}{\omega^2 - \omega_s^2} \right)^2 = 0 \tag{16}$$

where the two diagonal effective stiffness ratios κ_{tt} and κ_{pp} are determined by the direct EEMCF evaluated as in (14).

When shunts t and p are in OC, while the remaining shunts are in SC, the eigenvalue problem for the single shunt (B.5) is simply extended by adding the electrical stiffness from shunt p, leading to the eigenvalue problem (B.6) with natural frequency $\hat{\omega}_{n,tp}$ described by the double index tp to indicate that both shunts t and p are now in OC. The characteristic equation in (16) is established exactly in this limit, whereby the solution must be $\omega = \hat{\omega}_{s,tp}$. Hereby, the off-diagonal effective stiffness ratio κ_{tp} is the only unknown in (16), which can then be written in the quadratic polynomial form

$$\frac{K_{tp}^4}{\kappa_{tp}^2} - 2\frac{K_{tp}^2}{\kappa_{tp}} + \frac{K_{tp}^2}{K_{tt}^2} + \frac{K_{tp}^2}{K_{pp}^2} - \frac{K_{tp}^4}{K_{tt}^2 K_{pp}^2} = 0 \tag{17}$$

when the EEMCF

$$K_{tp}^2 = \frac{\hat{\omega}_{s,tp}^2 - \omega_s^2}{\omega_s^2} \tag{18}$$

is introduced similarly to the EEMCF K_{tt}^2 in (14). It can be shown that the quadratic equation (17) has two real-valued solutions for realistic EEMCFs of the shunts, when $K_{tp}^2 > K_{tt}^2$ and $K_{tp}^2 > K_{pp}^2$. Only the smaller of the two solutions is physical, whereby the effective reciprocal stiffness becomes

$$\frac{1}{\kappa_{tp}} = \frac{1}{K_{tp}^2} - \frac{1}{K_{tp}^2} \sqrt{\left(\frac{K_{tp}^2}{K_{pp}^2} - 1 \right) \left(\frac{K_{tp}^2}{K_{tt}^2} - 1 \right)} \tag{19}$$

It is noted that (19) implies symmetry ($\kappa_{tp} = \kappa_{pt}$) and recovers the expression for $1/\kappa_{tt}$ in (14) when $p = t$.

4 Proportional calibration

The governing equation in (10) for the piezoelectric shunt t, depends on all supplementary shunt forces, whereby the characteristic equation becomes infeasible because it is derived from the determinant of a set of P coupled equations. This multidimensionality is circumvented by imposing a proportionality between shunt forces, which reduces (10) to a single-shunt characteristic equation for which tuning expressions are readily available from the literature.

4.1 The OC shunt force

The governing equation (10) is derived from an expansion in SC mode shapes, for which f_p is zero for all shunts. In the opposite limit with all shunts in OC, the charge $Q_p = 0$, which corresponds to $Z_p \to \infty$, whereby (6) gives the shunt force

$$f_p = \frac{\theta_p^2}{C_p} \sum_{n=1}^{N} \nu_{n,p} r_n \tag{20}$$

An equivalent expression can be found for a mode shape expansion with all shunts in OC, where the corresponding natural angular frequencies and mode shape vectors are obtained from the eigenvalue problem (B.4). Thus, the contribution to the shunt force in the OC limit for the targeted mode $n = s$ is then defined as

$$\hat{f}_{s,p} = \frac{\theta_p^2}{C_p} \hat{\nu}_{s,p} \tag{21}$$

where the OC modal amplitude $\hat{\nu}_{s,p}$ at shunt location p is defined as in (B.3) for the corresponding SC limit. This OC modal shunt force amplitude $\hat{f}_{s,p}$ is now used to balance the individual shunt forces in (20) with respect to their respective OC values for target mode $n = s$.

4.2 Shunt force proportionality

The modal expansion is based on SC mode shapes, associated with no shunt forces. As the shunts are connected

to piezoelectric transducers at different locations along the structure, their individual sizing must account for any interaction of the shunts. The shunt forces are known in the OC limit case. Inspired by the sizing of viscous dampers in Main and Krenk (2005), a simple condition is used for the balancing of the shunts, which requires that they all reach the OC limit at the same rate when the impedance $Z_p \to \infty$ for $p = 1 \dots P$. This suggests the proportionality

$$\frac{f_p}{\hat{f}_{s,p}} = \frac{f_t}{\hat{f}_{s,t}} \tag{22}$$

between two shunts p and t. In the following, shunt t is assumed to be the targeted shunt that is calibrated by any preferred tuning principle, while the influence of the remaining shunts, here represented by shunt p, are then included according to the tuning of shunt t. Thus, from (22) the force by shunt p is isolated as

$$f_p = \frac{\hat{f}_{s,p}}{\hat{f}_{s,t}} f_t = \frac{C_t \theta_p^2}{C_p \theta_t^2} \frac{\hat{\nu}_{s,p}}{\hat{\nu}_{s,t}} f_t \simeq \frac{C_t \theta_p^2}{C_p \theta_t^2} \frac{\nu_{s,p}}{\nu_{s,t}} f_t \tag{23}$$

where the expression for the OC shunt force amplitude (21) is initially introduced, while the approximation $\hat{\nu}_{s,p} \simeq \nu_{s,p}$ is then used to secure subsequent expressions in which the particular sign of the target mode shapes becomes irrelevant as $\nu_{s,p}$ only appears squared.

When inserting the proportionality relation (23), the shunt force f_t can be extracted as a common coefficient, whereby the isolated equation for shunt t can be expressed from (10) in the compact form

$$\left(\frac{1}{\beta_t} + \frac{1}{i\omega} \frac{k_s}{\nu_{s,t}^2 \theta_t^2 Z_t} - \frac{\omega_s^2}{\omega^2 - \omega_s^2} \gamma_t \right) \frac{\nu_{s,t}}{k_s} f_t = 0 \tag{24}$$

when collecting the contributions from the other shunts $p \neq t$ in two coefficients β_t and γ_t, which are conveniently defined by the relations

$$\frac{1}{\beta_t} = \frac{1}{\kappa_{tt}} + \sum_{p \neq t}^{P} \frac{1}{\kappa_{tp}} \frac{\nu_{s,p}^2}{\nu_{s,t}^2} \frac{C_t \theta_p^2}{C_p \theta_t^2} \tag{25}$$

$$\gamma_t = 1 + \sum_{p \neq t}^{P} \frac{\nu_{s,p}^2}{\nu_{s,t}^2} \frac{C_t \theta_p^2}{C_p \theta_t^2} \tag{26}$$

The coefficient γ_t in (26) explicitly contains a correction for the interaction between shunts for the target mode $n = s$. The coefficient $1/\beta_t$ in (25) further implicitly introduces a correction for residual modes via the effective stiffness ratios κ_{tp}. A characteristic equation that governs the natural frequency ω is then directly obtained from the parenthesis in (24) as

$$\frac{1}{\beta_t \gamma_t} + \frac{1}{i\omega} \frac{1}{\gamma_t \nu_{s,t}^2} \frac{k_s}{\theta_t^2 Z_t} - \frac{\omega_s^2}{\omega^2 - \omega_s^2} = 0 \tag{27}$$

which is used to sequentially tune all shunts $t = 1 \dots P$. Thereby, the present force proportionality reduces the $P \times P$ determinant equation in (10) to a scalar characteristic equation for each of the P shunts in (27) that is feasible for shunt tuning. The only remaining parameter to be included in (27) is the shunt impedance Z_t, which makes the above characteristic equation applicable for calibration of general shunt architectures.

4.3 Equivalent lumped parameters

Calibration of the shunt impedance Z_t in (27) follows from comparison with the characteristic equation for the single-degree-of-freedom (sdof) lumped parameter model in Fig. 2, for which tuning expressions are readily available from the literature. In the sdof structure, mass m_s and stiffness k_s are the modal parameters for $n = s$ in (B.2), while the equivalent mechanical components

$$\bar{k} = \frac{\theta_t^2}{\bar{C}_t}, \quad \bar{c}(\omega) = \theta_t^2 \bar{Z}_t(\omega) \tag{28}$$

represent the lumped model capacitance $\bar{C}_t$ and impedance $\bar{Z}_t(\omega)$, respectively. The bar $\bar{(\,)}$ denotes equivalent parameters for the lumped sdof model. The equivalent sdof parameters are determined in the following from the already introduced physical parameters to allow sdof calibration expressions to be used for tuning of the shunts. Corresponding to the definition used e.g. by Park and Inman (1999), the EEMCF can for a shunted sdof system be defined as

$$\bar{K}_t^2 = \frac{\bar{k}}{k_s} = \frac{\theta_t^2}{\bar{C}_t k_s} \tag{29}$$

which determines the sdof capacitance $\bar{C}_t$ as function of the EEMCF $\bar{K}_t^2$, the actual piezoelectric coefficient θ_t^2 for the

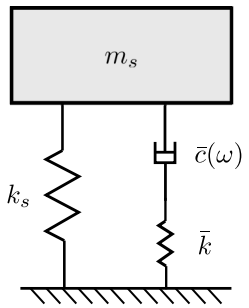

Figure 2. Lumped parameter representation with equivalent mechanical components of a single shunt.

Table 1. Calibration expressions for a single series RL-shunt attached to an sdof structure. Calibration methods are *PPM*: Pole placement method (Hagood and Von Flotow 1991) and *FPM*: Fixed point method (Yamada et al. 2010).

Label	$\omega_s^2 \bar{L}_t \bar{C}_t$	$\omega_s \bar{R}_t \bar{C}_t$
PPM	$\dfrac{1}{\left(1+\bar{K}_t^2\right)^2}$	$\sqrt{\dfrac{4\bar{K}_t^2}{\left(1+\bar{K}_t^2\right)^3}}$
FPM	$\dfrac{1}{1+\bar{K}_t^2}$	$\sqrt{\dfrac{3\bar{K}_t^2}{(2+\bar{K}_t^2)(1+\bar{K}_t^2)}}$

Table 2. Calibration of P shunts to mode $n = s$.

For each shunt $p = 1 \dots P$:
1. Piezoelectric parameters: C_p and θ_p.
2. Mode shape amplitude: $\nu_{s,p}$ from (B.3).
3. Calculate $1/\kappa_{tp}$ from (19) for $t = 1 \dots P$.

Tuning of shunt $t = 1 \dots P$:
4. Calculate γ_t and β_t from (25) and (26).
5. Sdof model: $\bar{K}_t^2 = \beta_t \gamma_t$, $\bar{C}_t = \theta_t^2/(\bar{K}_t^2 k_s)$.
6. Tuning: $\bar{L}_t$ and $\bar{R}_t$ from literature (e.g. Table 1).
7. Scaling: L_t and R_t by (32).

t'th piezoelectric transducer and the modal stiffness $k_s = \omega_s^2 m_s$ for the target mode $n = s$.

For the series RL shunt, two common tuning expressions for the sdof model are expressed in terms of $\bar{K}_t^2$ in Table 1. The characteristic equation for free vibrations of the lumped parameter sdof model in Figure 2 is established as

$$\frac{1}{\bar{K}_t^2} + \frac{1}{i\omega}\frac{k_s}{\bar{c}} - \frac{\omega_s^2}{\omega^2 - \omega_s^2} = 0 \tag{30}$$

The actual shunt components are then determined by equivalence between this equation for the sdof model and the characteristic equation (27) for shunt t acting on the full flexible structure. Initially, the EEMCF for the lumped parameter model

$$\bar{K}_t^2 = \beta_t \gamma_t \tag{31}$$

is found by comparison of the first terms in (30) and (27). Subsequently, the middle terms identify an expression for $\bar{c}$, which upon substitution of the second expression in (28) gives the direct impedance equivalence

$$Z_t = \frac{\bar{Z}_t}{\gamma_t \nu_{s,t}^2} \tag{32}$$

Thus, an actual component in Z_t is found by scaling the equivalent component in $\bar{Z}_t$ according to (32). The scaling explicitly accounts for shunt interaction (γ_t) and mode shape amplitude ($\nu_{s,t}^2$), while residual mode correction is indirectly included via $\bar{K}_t^2$ in (31). The full calibration procedure that corrects for residual modes and shunt interaction is outlined in Table 2.

5 Numerical examples

The aim of this section is to investigate the influence from residual modes and shunt interactions in the calibration of multiple piezoelectric shunts targeting a single vibration mode. Although this section only considers series RL shunts, the tuning method can be applied to any shunt architecture targeting a single mode.

The calibration is based on a consistent correction of calibration expressions for a single shunt targeting an sdof structure. Two different calibration principles are applied: maximum modal damping based on the pole placement method (PPM) by Hagood and Von Flotow (1991) and minimum response amplitude from the fixed point method (FPM) by Yamada et al. (2010). For these methods, Table 1 presents the non-dimensional inductance $\bar{L}$ and resistance $\bar{R}$ for a single series RL shunt attached to an sdof structure.

In the following, three different levels of correction are implemented and compared:

- **Individual**: $\beta_t = \kappa_{tt} = K_{tt}^2$ and $\gamma_t = 1$.
- **Reduced**: $\beta_t = \kappa_{tt} = K_{tt}^2$ and γ_t from (26).
- **Full**: β_t and γ_t from (25) and (26).

The full correction includes both residual mode correction and correction for shunt interactions. In the reduced correction, the diagonalization of $\beta_t = \kappa_{tt}$ neglects the influence of residual modes from other shunts. Thereby, shunt interaction is only included by the main targeted vibration mode, which makes the reduced correction similar to the correction used by Toftekær and Høgsberg (2020). Finally, the individual tuning furthermore omits the shunt interaction by $\gamma_t = 1$, although still including the residual mode correction for the considered shunt by $\beta_t = \kappa_{tt} = K_{tt}^2$. The individual correction uses the EEMCF for the calibration of each individual shunt; an approach often applied in the literature because it is easy to evaluate and takes device imperfections into account (Toftekær et al. 2018).

5.1 Primary test case

A primary test case is considered in terms of the free-free rod with 20 decentralized shunts in Figure 1, similar to numerical and experimental examples used by Lossouarn et al. (2015) and Trindade et al. (2021). Although the present method is applicable to more complex structures, such as beams and plates, the simple free-free rod is chosen as the numerical example, because results are comparably simple to replicate in laboratory experiments, see Lossouarn et al. (2015). The

rod is made of AU4G aluminium, has the length $L_r = 1000\,\mathrm{mm}$, width and thickness $b_r = h_r = 20\,\mathrm{mm}$, density $\rho_r = 2780\,\mathrm{kg\,m^{-3}}$ and Young's modulus $Y_r = 73.9\,\mathrm{GPa}$. Each shunted unit comprises a pair of PIC151 piezoelectric patches connected in parallel to an electrical circuit with impedance Z_t. All piezoelectric patches are identical with the length $L_{piezo} = 30\,\mathrm{mm}$, width $b_{piezo} = 20\,\mathrm{mm}$, thickness $h_{piezo} = 0.5\,\mathrm{mm}$, density $\rho_{piezo} = 7800\,\mathrm{kg\,m^{-3}}$, Young's modulus $Y^E_{piezo} = 66.7\,\mathrm{GPa}$ at zero electrical field, piezoelectric charge constant $d_{31} = -210\,\mathrm{pCN^{-1}}$ and dielectric permittivity $\epsilon^\sigma_{33} = 21.2\,\mathrm{nF\,m^{-1}}$. The spacing between the patches is $20\,\mathrm{mm}$, while the distance from the outer patches' end to the end of the rod is $10\,\mathrm{mm}$, see Trindade et al. (2021). In accordance to Trindade et al. (2021) and Lossouarn et al. (2015), the blocked capacitance for each piezoelectric shunt t is defined as $C_t = 35.2\,\mathrm{nF}$ and the piezoelectric coefficient is $\theta_t = 0.501\,\mathrm{N/V}$.

Structural damping is not included in the present study to highlight the effects of the piezoelectric shunts and the rod is modelled using the finite element method with 41 bar elements. The element mass and stiffness matrices are obtained using linear shape functions, corresponding to the matrices given for bar elements in Géradin and Rixen (2014).

The piezoelectric shunts are calibrated with respect to the first vibration mode with all shunts in SC. This corresponds to the target frequency $\omega_s = \omega_1 = 15766\,\mathrm{rad/s}$ for mode $s = 1$. The EEMCF for each shunt in SC/OC with all other shunts in SC increases from $K^2_{1\,1} = K^2_{20\,20} = 2.50 \cdot 10^{-6}$ for the two outer pair of patches (close to the ends of the rod) to $K^2_{10\,10} = K^2_{11\,11} = 4.03 \cdot 10^{-4}$ for the two pair of patches next to the center of the rod.

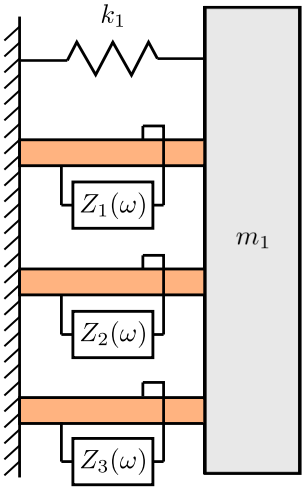

Figure 3. Simplified test case in terms of an sdof system with three shunts.

5.2 Frequency response

The frequency response for an external harmonic load is determined for the primary test case of the free-free rod with 20 shunts. Furthermore, to highlight the influence of residual modes on the calibration, the frequency response is also determined for the simplified test case in Figure 3 with three shunts attached to an sdof structure. The mass and stiffness of the sdof structure are chosen to correspond to the free-free rod with shunt 10 used for damping of target mode $s = 1$ and the other shunts in SC. Thus, the sdof mass $m_s = m_1 = 70.8\,\mathrm{kg}$ and stiffness $k_s = k_1 = 1.76 \cdot 10^{10}\,\mathrm{N/m}$ are derived from (B.2) for the free-free rod model with unit deflection along the considered patch 10, i.e. $\mathbf{w}^T_{10}\mathbf{u}_s = 1$. Thereby, the natural frequency of the sdof structure and EEMCF of the shunt correspond to the values obtained for the free-free rod with shunt 10 used for vibration damping. Three patches are attached to the sdof mass to include the effect of shunt interaction. The piezoelectric properties of the three patches are equal to the considered patch 10 of the free-free rod. For the free-free rod, the load is considered as a point load at the

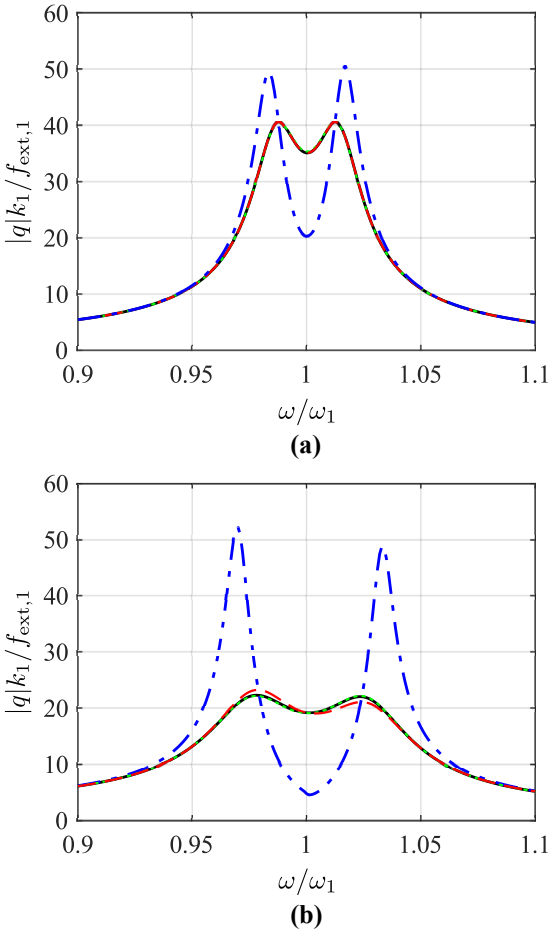

Figure 4. Frequency response curves: sdof structure with three shunts **(a)** and free-free rod with 20 shunts **(b)**. Correction: *individual* (blue dashed-dotted), *reduced* (red dashed), and *full* (black solid). Numerical optimum tuning (green dotted).

left tip of the rod, while for the sdof structure, the load acts directly on the mass m_1.

For the frequency response analysis, the shunts are tuned by the Fixed-Point Method (FPM) in Table 1. The frequency response curves are shown in Figure 4 for the sdof structure with three shunts in (a) and the free-free rod with 20 shunts in (b). In each sub-figure, the three different levels of correction are represented by: black solid, red dashed, and blue dashed-dotted curves, respectively. The green dotted curves represent the absolute optimum with identical shunt parameters, obtained by a simple search algorithm (`fminsearch` in Matlab) that minimizes the maximum response amplitude in the frequency curve around the targeted natural frequency.

Table 3 presents the maximum frequency amplitude around the targeted resonance ω_1 for all combinations of the three corrections (full, reduced, and individual) for both the sdof structure and the free-free rod. All six amplitudes are divided by the maximum frequency amplitude from (dotted) curves obtained by the numerical optimization.

The shunt tuning obtained with full, reduced, and individual correction, as well as by the numerical optimum, are summarized in Table 4. For the sdof structure with three shunts, all shunts have identical tuning for L_t and R_t because their patches have identical C_t and θ_t. For the primary test case, where the 20 piezoelectric patch pairs are placed differently on the free-free rod, the tuning for each shunt is in principle different. However, the present tuning yields practically identical shunt components, in Table 4 represented by a mean value and a corresponding standard deviation, which almost vanishes for the full correction. Therefore, the numerical optimization (dotted) assumes identical L_t and R_t for all 20 shunts.

5.2.1 Simplified test case The sdof structure with three shunts includes the influence from shunt interaction, whereby the individual correction (blue dashed-dotted) curve exhibits a substantial amplitude increase in Figure 4(a), which in Table 3 becomes almost 25% larger than the numerical optimum.

Because residual modes are not present for the sdof structure, the reduced (red dashed) and full correction (black solid) result in identical tuning in Table 4 and almost recover the numerical optimum in Figure 4(a) and Table 3. Furthermore, the response with two peaks of equal magnitude for the reduced and full correction is similar to the expected response for the FPM calibration with a single shunt in Yamada et al. (2010). The simplified test case results show that the reduced correction, with a diagonalized $\kappa_{tt} = K_{tt}^2$, is very accurate when the influence from residual modes is insignificant.

Table 3. Ratio of maximum displacement for the FPM with individual, reduced, or full correction, relative to the numerical calibration. For the free-free rod $\max(K_{nn}) = 0.020$, while uniform scaling of the shunt capacitance gives $\max(K_{nn}) = 0.050$ (*) and $\max(K_{nn}) = 0.100$ (**).

	Individual	Reduced	Full
Sdof structure	1.2459	1.0004	1.0004
Free-free rod	2.3599	1.0486	1.0056
Free-free rod*	2.5085	1.1214	1.0139
Free-free rod**	2.8239	1.2517	1.0326

Table 4. Calibration parameters for the FPM. The parameters are represented by the mean and standard deviation for the free-free rod with 20 shunts.

Sdof structure	L_t [mH]	R_t [Ω]
Individual	114.4	44.50
Reduced	114.3	77.02
Full	114.3	77.02
Numerical	114.3	77.59
Free-free rod	L_t [mH]	R_t [Ω]
Individual	$113.6 \pm 6.0 \cdot 10^{-3}$	$28.16 \pm 1.4 \cdot 10^{1}$
Reduced	$113.2 \pm 1.8 \cdot 10^{-2}$	$139.3 \pm 3.3 \cdot 10^{-2}$
Full	$113.6 \pm 5.1 \cdot 10^{-5}$	$140.2 \pm 9.4 \cdot 10^{-5}$
Numerical	113.7	139.7

5.2.2 Primary test case The free-free rod with 20 shunts includes effects from both residual modes and shunt interaction. Thus, the individual correction (blue dashed-dotted) introduces two very high resonance peaks in Figure 4(b). Furthermore, the influence from residual modes implies that the reduced correction (red dashed) exhibits a minor response amplification compared to the full correction (black solid), which coincides with the numerical optimum (dotted). The detuning observed for the reduced correction is caused by the slightly smaller inductance L_t in Table 4, in which the mean value (113.2 mH) differs by 0.4% compared to the numerical optimum (113.7 mH). The accuracy of the full correction is further validated by the maximum amplitude ratio in Table 3, where the 0.56% increase for the full correction is about one-tenth of the 4.86% increase by the reduced correction. The results for the free-free rod demonstrate that shunt tuning based on the proposed (full) correction accounts very accurately for both modal spill-over from residual modes as well as the interaction between shunts.

To further investigate the ability of the proposed (full) correction to consistently account for shunt interaction, the EEMCF is increased to amplify the influence from the other shunts. For the individual shunts, used to obtain the previous

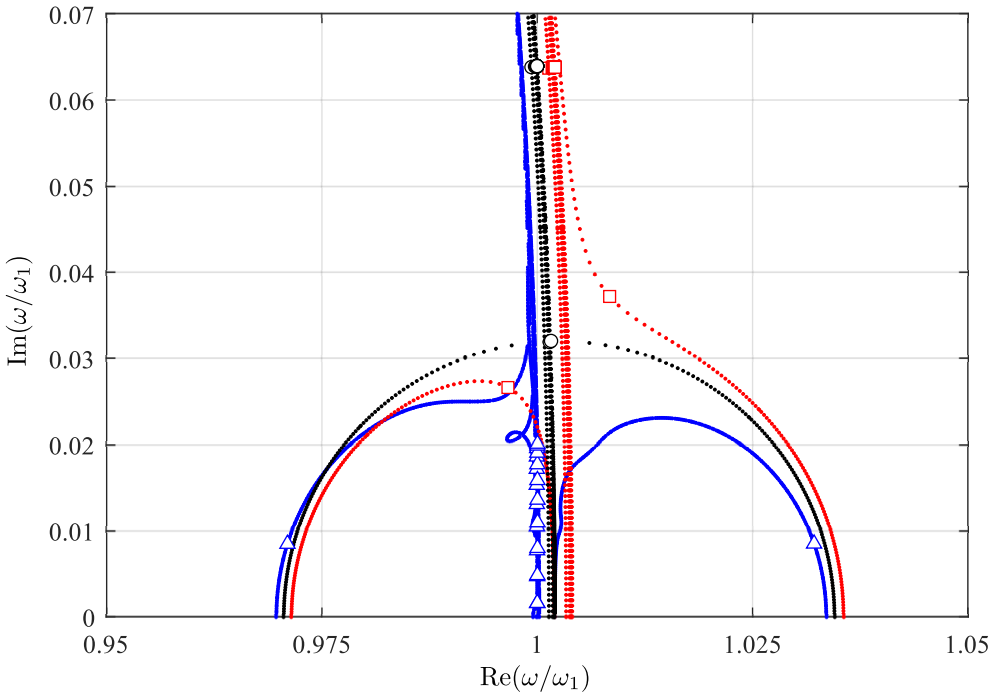

Figure 5. Root locus diagram for the free-free rod with 20 shunts for the PPM. The triangles (△), squares (□), and circles (○) represent the PPM tuning for the corrections: *individual* (blue), *reduced* (red), and *full* (black), respectively.

curves in Figure 4(b), the largest value of the square root of the EEMCF is $\max(K_{nn}) = 0.02$ for the free-free rod. However, larger values can be found in the literature, e.g. 0.14 for a beam with a single patch on both sides in Thomas et al. (2009) and Thomas et al. (2012), or 0.16 in Hagood and Von Flotow (1991). Alternatively, the EEMCF can be increased by the addition of a negative shunt capacitance (De Marneffe and Preumont 2008). Table 3 includes the maximum amplitude ratios for two alternative cases, in which the blocked capacitance is scaled by a factor of 0.1555 (*) and 0.0340 (**). This reduction in capacitance yields a corresponding increase in $\max(K_{nn})$ from 0.02 (for the original patch pairs) to 0.05 and 0.100. As seen in Table 3, this increase in EEMCF yields an amplification of the maximum amplitude ratio by up to 25% for the reduced correction, while the full correction limits the amplification to 3%. This example with larger EEMCF illustrates the improvement obtained by the present inclusion of residual modes in the terms accounting for the interaction between shunts.

5.3 Root locus analysis

The root locus diagrams in Figure 5 are determined for the free-free rod with the 20 shunts tuned by the Pole Placement Method (PPM) in Table 1. The complex poles ω are governed by the eigenvalue problem introduced in Appendix A. The root trajectories in Figure 5 are then obtained by solving this eigenvalue problem for different scaling of the optimal resistance determined by the PPM, i.e. using $R_t = \alpha R_t^{PPM}$ for each shunt with α from 0 to ∞. The three root locus diagrams in Figure 5 are obtained for the individual correction (blue), reduced correction (red) and full correction (black).

As shown in Hagood and Von Flotow (1991) for an sdof structure, the PPM tuning of a single shunt forms a half circle, which merges with a backbone circle at a bifurcation point. By the full correction (black) in Figure 5, the desired root locus structure is recovered for target mode $s = 1$ of the free-free rod. The large circles (○) depict the complex roots exactly at the PPM tuning ($\alpha = 1$). Two of the 21 complex poles (○) form a double root exactly at the bifurcation point, while the remaining redundant poles are heavily damped because they are located beyond the bifurcation point along the backbone trajectory.

For the reduced correction (red, □) in Figure 5, the redundant poles are still heavily damped, while the two critical modes do not exactly form a double root that meet at a bifurcation point. This results in a slight reduction in attainable damping compared to the desired tuning with full correction.

The importance of consistently including shunt and modal interaction is illustrated for the PPM tuning with individual correction (blue) in Figure 5. The two critical roots along the semi-circular trajectories are far away from the apparent bifurcation point, while the remaining redundant poles are

now placed well below the bifurcation point and thus almost undamped for the triangles (△) closest to the real axis.

6 Conclusion

This paper describes the influence of both residual modes and shunt interaction on the tuning of multiple piezoelectric shunts targeting a single vibration mode. This results in explicit correction terms that can be used for calibration of the shunts based on available tuning expressions developed for a single shunt attached to an undamped sdof structure.

The shunt interaction and the influence from residual modes are included by the introduction of effective stiffness ratios, which are then determined from EEMCFs. The effective stiffness ratios are combined with a prescribed force ratio, corresponding to all shunts in OC. This results in a single characteristic equation on scalar form, which represents an equivalent sdof model that can be used for explicit calibration of each shunt.

The accuracy of the proposed calibration method has been validated numerically for series RL shunts by comparison of the frequency response curves and root locus diagrams for different levels of correction. When the calibration is conducted for series RL shunts based on the fixed point method for minimum displacement, it is found that the calibration is practically similar to a numerical calibration with equal parameters for all shunts.

Funding

This research received no specific grant from any funding agency in the public, commercial, or not-for-profit sectors.

Declaration of conflicting interests

The Authors declare that there is no conflict of interest.

References

Abé M and Fujino Y (1994) Dynamic characterization of multiple tuned mass dampers and some design formulas. *Earthquake Engineering & Structural Dynamics* 23(8): 813–835.

Airoldi L and Ruzzene M (2011) Design of tunable acoustic metamaterials through periodic arrays of resonant shunted piezos. *New Journal of Physics* 13(11): 113010.

Andreaus U and Porfiri M (2007) Effect of electrical uncertainties on resonant piezoelectric shunting. *Journal of Intelligent Material Systems and Structures* 18(5): 477–485.

Berardengo M, Manzoni S, Vanali M et al. (2016a) The behaviour of mistuned piezoelectric shunt systems and its estimation. *Shock and Vibration* 2016.

Berardengo M, Thomas O, Giraud-Audine C and Manzoni S (2016b) Improved resistive shunt by means of negative capacitance: new circuit, performances and multi-mode control. *Smart Materials and Structures* 25(7): 075033.

Caruso G (2001) A critical analysis of electric shunt circuits employed in piezoelectric passive vibration damping. *Smart Materials and Structures* 10(5): 1059.

Casadei F, Ruzzene M, Dozio L and Cunefare K (2009) Broadband vibration control through periodic arrays of resonant shunts: experimental investigation on plates. *Smart Materials and Structures* 19(1): 015002.

De Marneffe B and Preumont A (2008) Vibration damping with negative capacitance shunts: theory and experiment. *Smart Materials and Structures* 17(3): 035015.

Forward RL (1979) Electronic damping of vibrations in optical structures. *Applied Optics* 18(5): 690–697.

Gardonio P and Casagrande D (2017) Shunted piezoelectric patch vibration absorber on two-dimensional thin structures: Tuning considerations. *Journal of Sound and Vibration* 395: 26–47.

Géradin M and Rixen DJ (2014) *Mechanical vibrations: theory and application to structural dynamics*. John Wiley & Sons.

Gripp J and Rade D (2018) Vibration and noise control using shunted piezoelectric transducers: A review. *Mechanical Systems and Signal Processing* 112: 359–383.

Hagood NW and Von Flotow A (1991) Damping of structural vibrations with piezoelectric materials and passive electrical networks. *Journal of Sound and Vibration* 146(2): 243–268.

Hoffmeyer D and Høgsberg J (2020) Calibration and balancing of multiple tuned mass absorbers for damping of coupled bending-torsion beam vibrations. *Journal of Vibration and Acoustics* 142(4): 044501.

Høgsberg J and Krenk S (2012) Balanced calibration of resonant shunt circuits for piezoelectric vibration control. *Journal of Intelligent Material Systems and Structures* 23(17): 1937–1948.

Høgsberg J and Krenk S (2015) Balanced calibration of resonant piezoelectric rl shunts with quasi-static background flexibility correction. *Journal of Sound and Vibration* 341: 16–30.

Høgsberg J and Krenk S (2017) Calibration of piezoelectric rl shunts with explicit residual mode correction. *Journal of Sound and Vibration* 386: 65–81.

Igusa T and Xu K (1994) Vibration control using multiple tuned mass dampers. *Journal of Sound and Vibration* 175(4): 491–503.

Ikegame T, Takagi K and Inoue T (2019) Exact solutions to h∞ and h2 optimizations of passive resonant shunt circuit for electromagnetic or piezoelectric shunt damper. *Journal of Vibration and Acoustics* 141(3): 031015.

Krenk S and Høgsberg J (2014) Tuned mass absorber on a flexible structure. *Journal of Sound and Vibration* 333(6): 1577–1595.

Krenk S and Høgsberg J (2016) Tuned resonant mass or inerter-based absorbers: unified calibration with quasi-dynamic flexibility and inertia correction. *Proceedings of the Royal Society A: Mathematical, Physical and Engineering Sciences* 472(2185): 20150718.

Lossouarn B, Aucejo M and Deü JF (2015) Multimodal coupling of periodic lattices and application to rod vibration damping with a piezoelectric network. *Smart Materials and Structures* 24(4): 045018.

Main JA and Krenk S (2005) Efficiency and tuning of viscous dampers on discrete systems. *Journal of Sound and Vibration* 286(1-2): 97–122.

Park CH and Inman DJ (1999) Uniform model for series rl and parallel rl shunt circuits and power consumption. In: *Smart Structures and Materials 1999: Smart Structures and Integrated Systems*, volume 3668. SPIE, pp. 797–804.

Preumont A (2018) *Vibration control of active structures: an introduction*, volume 246. Springer.

Raze G, Dietrich J, Lossouarn B and Kerschen G (2022) Shunts vs networks: tuning and comparison of centralized and decentralized piezoelectric vibration absorbers. *Smart Materials and Structures* 31(11): 115006.

Richardt JD, Høgsberg J, Lossouarn B and Deü JF (2023) Analysis and tuning of multiple shunted piezoelectric transducers. In: *Proceedings of the 10th International Conference on Smart Structures and Materials, Patras, Greece, 3-5 July 2023*. Eccomas Proceedia, pp. 191–202.

Soltani P, Kerschen G, Tondreau G and Deraemaeker A (2014) Piezoelectric vibration damping using resonant shunt circuits: an exact solution. *Smart Materials and Structures* 23(12): 125014.

Soltani P, Kerschen G, Tondreau G and Deraemaeker A (2017) Tuning of a piezoelectric vibration absorber attached to a damped structure. *Journal of Intelligent Material Systems and Structures* 28(9): 1115–1129.

Thomas O, Deü JF and Ducarne J (2009) Vibrations of an elastic structure with shunted piezoelectric patches: efficient finite element formulation and electromechanical coupling coefficients. *International Journal for Numerical Methods in Engineering* 80(2): 235–268.

Thomas O, Ducarne J and Deü JF (2012) Performance of piezoelectric shunts for vibration reduction. *Smart Materials and Structures* 21(1): 015008.

Thorp O, Ruzzene M and Baz A (2001) Attenuation and localization of wave propagation in rods with periodic shunted piezoelectric patches. *Smart Materials and Structures* 10(5): 979.

Toftekær JF, Benjeddou A, Høgsberg J and Krenk S (2018) Optimal piezoelectric resistive–inductive shunt damping of plates with residual mode correction. *Journal of Intelligent Material Systems and Structures* 29(16): 3346–3370.

Toftekær JF and Høgsberg J (2020) Multi-mode piezoelectric shunt damping with residual mode correction by evaluation of modal charge and voltage. *Journal of Intelligent Material Systems and Structures* 31(4): 570–586.

Trindade MA, Lossouarn B and Deü JF (2021) Effect of parametric uncertainties on vibration mitigation with periodically distributed and interconnected piezoelectric patches. *Journal of Intelligent Material Systems and Structures* 32(9): 971–985.

Wu Sy (1996) Piezoelectric shunts with a parallel rl circuit for structural damping and vibration control. In: *Smart Structures and Materials 1996: Passive Damping and Isolation*, volume 2720. Spie, pp. 259–269.

Yamada K, Matsuhisa H, Utsuno H and Sawada K (2010) Optimum tuning of series and parallel lr circuits for passive vibration suppression using piezoelectric elements. *Journal of Sound and Vibration* 329(24): 5036–5057.

Yang F, Sedaghati R and Esmailzadeh E (2022) Vibration suppression of structures using tuned mass damper technology: A state-of-the-art review. *Journal of Vibration and Control* 28(7-8): 812–836.

Appendix A

This appendix considers the modelling of a mechanical structure with P piezoelectric elements using the finite element method, see e.g. Preumont (2018); Thomas et al. (2009) for further details. In the frequency domain, the structural equation of motion (without damping) can be written as

$$\left(-\omega^2\mathbf{M}+\mathbf{K}\right)\mathbf{q}+\sum_{p=1}^{P}\mathbf{w}_p f_p=\mathbf{f}_{\text{ext}} \tag{A.1}$$

where the vector $\mathbf{q}$ contains the generalized displacements, $\mathbf{M}$ is the mass matrix, $\mathbf{K}$ is the stiffness matrix, $\mathbf{f}_{\text{ext}}$ contains external loads and $\mathbf{w}_p$ is the connectivity vector that describes where the force f_p acts on the structure. The mass of the piezoelectric transducers are included in $\mathbf{M}$, while $\mathbf{K}$ contains their mechanical stiffness with SC electrodes.

The charge Q_p at the electrodes of shunt p is governed by the sensor or balance equation

$$Q_p=\theta_p\mathbf{w}_p^T\mathbf{q}+C_pV_p \tag{A.2}$$

in which the shunt capacitance C_p is associated with blocked transducer boundaries.

Upon elimination of V_p and Q_p by substitution of (4) and (5), the balance equation (A.2) can be written as

$$\left(\frac{C_p}{\theta_p^2}+\frac{1}{i\omega}\frac{1}{\theta_p^2 Z_p}\right) f_p = \mathbf{w}_p^T \mathbf{q} \tag{A.3}$$

which represents a mechanical force-displacement relationship for the p'th piezoelectric shunt.

The complex poles ω, describing the root locus diagram in Figure 5, are determined by solving the eigenvalue problem comprised by the homogeneous form of (A.1) and (A.3).

Appendix B

When all shunts are in SC, $V_p = 0$ for $p = 1, \ldots, P$ which implies that $f_p = 0$ in (4). The structural equation of motion in (A.1) then reduces to the eigenvalue problem

$$\left(-\omega_n^2 \mathbf{M} + \mathbf{K}\right) \mathbf{u}_n = \mathbf{0} \tag{B.1}$$

for a mode n, which governs the SC natural angular frequency ω_n and the corresponding mode shape vector $\mathbf{u}_n$. The associated modal parameters are

$$m_n = \mathbf{u}_n^T \mathbf{M} \mathbf{u}_n \ , \quad k_n = \mathbf{u}_n^T \mathbf{K} \mathbf{u}_n \tag{B.2}$$

while the deformation of the mode shape across the transducer location is defined by the parameter

$$\nu_{n,p} = \mathbf{u}_n^T \mathbf{w}_p = \mathbf{w}_p^T \mathbf{u}_n \tag{B.3}$$

with the indices referring to mode n and shunt p.

When all shunts $p = 1 \ldots P$ are in OC, then f_p in (A.1) is substituted from (A.3) with $Z_p \to \infty$, which yields the eigenvalue problem

$$\left(-\hat{\omega}_n^2 \mathbf{M} + \mathbf{K} + \sum_{p=1}^{P} \mathbf{w}_p \mathbf{w}_p^T \frac{\theta_p^2}{C_p}\right) \hat{\mathbf{u}}_n = \mathbf{0} \tag{B.4}$$

where $\hat{\mathbf{u}}_n$ and $\hat{\omega}_n$ denote respectively the mode shape and natural frequency with all P shunts in OC.

The natural frequency associated with shunt t in OC and the remaining shunts in SC is determined by solving the eigenvalue problem

$$\left(-\hat{\omega}_{n,tt}^2 \mathbf{M} + \mathbf{K} + \mathbf{w}_t \mathbf{w}_t^T \frac{\theta_t^2}{C_t}\right) \hat{\mathbf{u}}_{n,tt} = \mathbf{0} \tag{B.5}$$

which corresponds to (B.4) with $p = t$ as the single term in the summation.

In the final case, where two shunts t and p are in OC, while the remaining shunts are in SC, the eigenvalue problem

$$\left(-\hat{\omega}_{n,tp}^2 \mathbf{M} + \mathbf{K} + \mathbf{w}_t \mathbf{w}_t^T \frac{\theta_t^2}{C_t} + \mathbf{w}_p \mathbf{w}_p^T \frac{\theta_p^2}{C_p}\right) \hat{\mathbf{u}}_{n,tp} = \mathbf{0} \tag{B.6}$$

is simply obtained from (B.5) by adding the extra term for shunt p.